Hydrogen trapping by VC precipitates and structural defects in a high strength Fe–Mn–C steel studied by small-angle neutron scattering

B. Malard [a,*], B. Remy [b], C. Scott [b], A. Deschamps [a], J. Chêne [c], T. Dieudonné [b,c], M.H. Mathon [d]

[a] SIMaP, INP Grenoble – CNRS – UJF, BP 75, 38402 St Martin d'Hères Cedex, France
[b] ArcelorMittal (R&D Automotive Products), Voie Romaine, 57280 Maizières-les-Metz, France
[c] CEA/CNRS: "Hydrogène/Matériaux de structure", UMR 8587, 91191 Gif sur Yvette, France
[d] Laboratoire Léon Brillouin, CEA/Saclay, 91191 Gif sur Yvette Cedex, France

A B S T R A C T

The trapping of hydrogen by VC precipitates and structural defects in high strength Fe–Mn–C steel was studied by small angle neutron scattering. No interaction between H and V in solid solution has been detected but a significant interaction between H and structural defects introduced by plastic deformation has been measured. This last effect was reversible upon outgassing of the H. Moreover a significant interaction between H and VC precipitates has been measured; 5 ppm wt. of H could be trapped in the precipitates. This is consistent with the homogeneous trapping of H within the precipitates rather than at the precipitate/matrix interface.

Keywords:
Small-angle neutron scattering
Hydrogen embrittlement
Hydrogen trapped by nanoprecipitates

1. Introduction

Fe–Mn–C austenitic steels that exhibit the twinning induced plasticity (TWIP) effect are very attractive materials solutions for weight reduction of crash-resistant parts in new passenger vehicle developments, due to their combination of extremely high energy absorbing capacity coupled with large residual elongation after forming [1–6].

The combination of very high tensile strength (typically >1000 MPa) coupled with extended formability inevitably leads to the presence of regions of high levels of internal stresses after cold forming operations. If the concentration of mobile atomic hydrogen (H) in these zones exceeds a critical limit, the material can be susceptible to delayed cracking [7]. H content in the steel can be rigorously controlled at the production stage but mobile H may be introduced at later stages by welding, surface or heat treatments, corrosion, etc. It is thus advantageous to introduce H trapping sites in the microstructure that can act as sinks for mobile H and hence reduce the risk of delayed cracking. It is now appreciated that the addition of small amounts of vanadium (V) can reduce the severity of delayed cracking caused by the presence of mobile H [8] while at the same time enhancing the mechanical properties [9]. However, the physical interactions between mobile H and V either in solid solution or in the form of vanadium carbides (VC) precipitates in austenitic TWIP steels need to be studied in order to increase our understanding of the trapping process.

It is not easy to experimentally detect hydrogen in steels because of its high mobility and low solubility. Therefore, the understanding of hydrogen behaviour including diffusion and trapping has been limited due to the lack of suitable monitoring tools [10]. Thermal desorption analysis (TDA) is usually used to determine the hydrogen desorption characteristics, giving useful information about trapping sites and mobile hydrogen content over the entire specimen [11–14]. TDA is often used in conjunction with electrochemical permeation techniques (EP) which provide complementary information about diffusion coefficients [15,16]. However, information about the state, number and distribution of hydrogen atoms within the sample are still uncertain.

Techniques involving neutron scattering are among the most suitable tools for obtaining information on H distribution because neutrons have the advantage of a high sensitivity to light elements like hydrogen. Neutron scattering techniques are appropriate for measuring microstructures in the scale range from sub-angstrom (neutron diffraction) [17] to millimetre level (neutron radiography) [18,19]. In particular, small angle neutron scattering (SANS) is an appropriate technique for detecting H interactions with nanoscale microstructural features. For example, Ross et al. [20] and Maxelon et al. [21] have used this technique in Pd alloys to reach a consistent description of the interaction between hydrogen and dislocations. In addition, Kluthe et al. reported detection of H

* Corresponding author. Tel.: +33 04 76 82 66 69; fax: +33 04 76 82 66 44.
E-mail address: benoit.malard@simap.grenoble-inp.fr (B. Malard).

segregation at the internal interface of Ag/MgO using SANS [22]. They showed clear differences in the scattering profiles between H or deuterium (D) charged and uncharged samples. In situations with lower H concentrations, a difference in neutron scattering profiles can also be observed between H-charged and uncharged steels. Ulbricht et al., using SANS, reported that the behaviour of H trapped in the microstructural heterogeneities of a pressure vessel steel was mainly correlated with irradiation effects [23]. Recently, a Japanese team at NIMS has applied SANS techniques to the detection of H trapped by niobium carbides (NbC) in ferritic steels [24]. The neutron scattering intensity from nanometre scale NbC precipitates appears to be higher in the case of H-charged samples. If the same samples are then heated to outgas H the enhanced scattering intensity disappears. The authors claim that this effect is caused by the segregation or trapping of H at the NbC/ferrite interface.

H also interacts with lattice defects such as vacancies, dislocations and stacking faults. For example the trapping of H by dislocations and ε martensite has been observed experimentally by tritium autoradiography on austenitic stainless steels by Chêne et al. [25]. An indirect demonstration of the phenomenon of trapping is given by the decrease in the apparent H diffusion coefficient when the material is plastically deformed [26]. The peculiarity of H trapping at dislocations lies in the fact that these traps are mobile and can therefore assist the mechanism of H diffusion. The important role of mobile traps for the transport of H was first proposed by Bastien and Azou [27] 50 years ago. This transport mechanism was experimentally demonstrated by Donovan [28] by measuring the flow of tritium desorption introduced in tensile specimens. Recently, new observations conducted by Chêne and Brass [29–31] were used to quantify changes in the amount of tritium desorbed during a tensile test performed on a single crystal of nickel-based superalloy [30].

In this present work, to shed light on the interaction between H and nanoscale VC precipitates as well as other structural defects such as stacking faults, twins and dislocations, SANS and TDS were employed to investigate two TWIP steel compositions; a V-free steel, and a V-containing steel where the V was either in solid solution or in the form of precipitates. The effect of lattice defects was investigated by comparing samples with different degrees of cold rolling. Measurements were carried out with and without H charging.

2. Materials and techniques

The measured specimens were in the form of 1.2 mm cold strips prepared with three different microstructures (see Table 1 for alloy compositions).

The first microstructure (A) was a reference alloy with no V additions in a fully recrystallised state. The second (B) uses the same base composition modified by the addition of 0.215 wt.% V. It was studied in the full hard state (cold rolled with 50% reduction) where all V is in solid solution (validated by selective chemical dissolution) and containing a high density of crystalline defects (dislocations, twins and stacking faults). The third specimen, (C) was identical to (B) except recrystallisation annealed with 60% of the available V precipitated as spherical shape VC [9].[1] Different H charging and outgassing cycles were applied to these microstructures.

Table 1
Composition of the austenitic steels in %wt.

	C	Mn	Si	P	N	V
Sample (A)	0.585	18.4	0.195	0.032	0.020	0
Samples (B) and (C)	0.600	18.14	0.185	0.032	0.016	0.215

The processing cycle for the three microstructures was the following. After reheating (1180 °C – 15 min) the cast ingots were hot rolled to 2.4 mm and water quenched from above 900 °C. The samples were then chemically stripped (HCl bath), and cold rolled with a reduction rate of 50% to 1.2 mm. At this step the reference (B) with V in solid solution finished its processing cycle. The microstructures (A and C) were annealed at 800 °C for 180 s to form semi-coherent VC with an average precipitate diameter of 7–8 nm [9,32] (C) and a fully recrystallised microstructure (A and C).

Samples 12 mm × 12 mm in area were mechanically thinned and cathodically charged with H in 0.1 M aqueous NaOH solution. Two series of charging experiments were carried out, resulting in very different H concentrations and distribution (see Table 2 for details on sample thickness and charging conditions). In the moderate H charging conditions (18 °C, 24 h), assuming that the apparent diffusion coefficient of H at room temperature is about $D_{RT} = 10^{-12}$ cm^2 s^{-1} [33], the H concentration profile is expected to extend over about 10 μm on both sides of the sample thickness (500 μm). This corresponds to a non homogeneous distribution of H in the specimen and a low average concentration. In the severe H charging conditions (80 °C, 62 h), according to the experimental value of the apparent diffusion coefficient at 80 °C in Fe–Mn–C TWIP steels [34], the H concentration profile extends about 100 μm on both sides of the sample thickness (200 μm), resulting in a more homogeneous hydrogenation and a higher average concentration. Moreover short-circuit diffusion of H along grain boundaries may slightly enhance H absorption [34]. Immediately after H charging, the samples were stored in liquid nitrogen to prevent H desorption before SANS measurement.

The total H content was measured with the melt extraction technique. The sample is melted in a crucible and the hydrogen is extracted using an inert carrier gas pulse (argon). The signal generated by the thermal conductivity analyser is integrated to calculate the concentration by weight of the sample. The sensitivity of this technique is about 0.1 ppm wt.; it was not possible to give a standard deviation on the concentration values because lack of material meant that too few measurements could be made on hydrogenated samples.

SANS experiments were performed on the PAXY instrument at the Laboratoire Léon Brillouin (LLB) in Saclay, France. Neutrons are monochromated by a velocity selector to a mean wavelength of 6 Å and 9.5 Å, the wavelength spread being $\delta\lambda/\lambda = 9\%$. This wavelength was chosen in order to avoid double diffraction problems that can arise from the austenite microstructure. Sample–detector distances of 1.865 m and 6.065 m were used with the wavelength of 6 Å and 9.5 Å with appropriate collimation settings to give access to scattering vectors Q ($Q = 4\pi \sin\theta/\lambda$) ranging from 0.06 Å^{-1} to 0.2 Å^{-1}. The diameter of the neutron beam was 8 mm. Data processing was carried out using the GRASP software developed by C. Dewhurst at the Institute Laue Langevin (ILL). Data files were corrected for electronic noise, detector response and background noise, and normalised using a water standard. The Laue intensity was subtracted for all the presented data.

3. Results

3.1. Microstructural observations

Sample A consisted of fully recrystallised austenite with a grain size of 4–5 μm. No precipitates were detected by TEManalysis.

[1] In fact most precipitates were V(C,N) with the C content > V content.

Table 2
Concentration in H (ppm wt) of the different samples used for SANS experiments. B_{chg} or C_{chg} means charged sample. B_{out} means outgassed sample B at 260 °C during 24 h. C_{out} means outgassed sample C at 150 °C during 16 h.

Microstructure	No H charging	Moderate H charging 0.5 mm; 24 h; 18 °C; 1 mA/cm^2	Severe H charging 0.2 mm; 62 h; 80 °C; 50 mA/cm^2
(A) No vanadium	<1.5		
(B) V in solid solution	1.9	B_{chg}: 2.5 B_{out}: 0.8	
(C) VC precipitates	0.7		C_{chg}: 72 C_{out}: 11.5

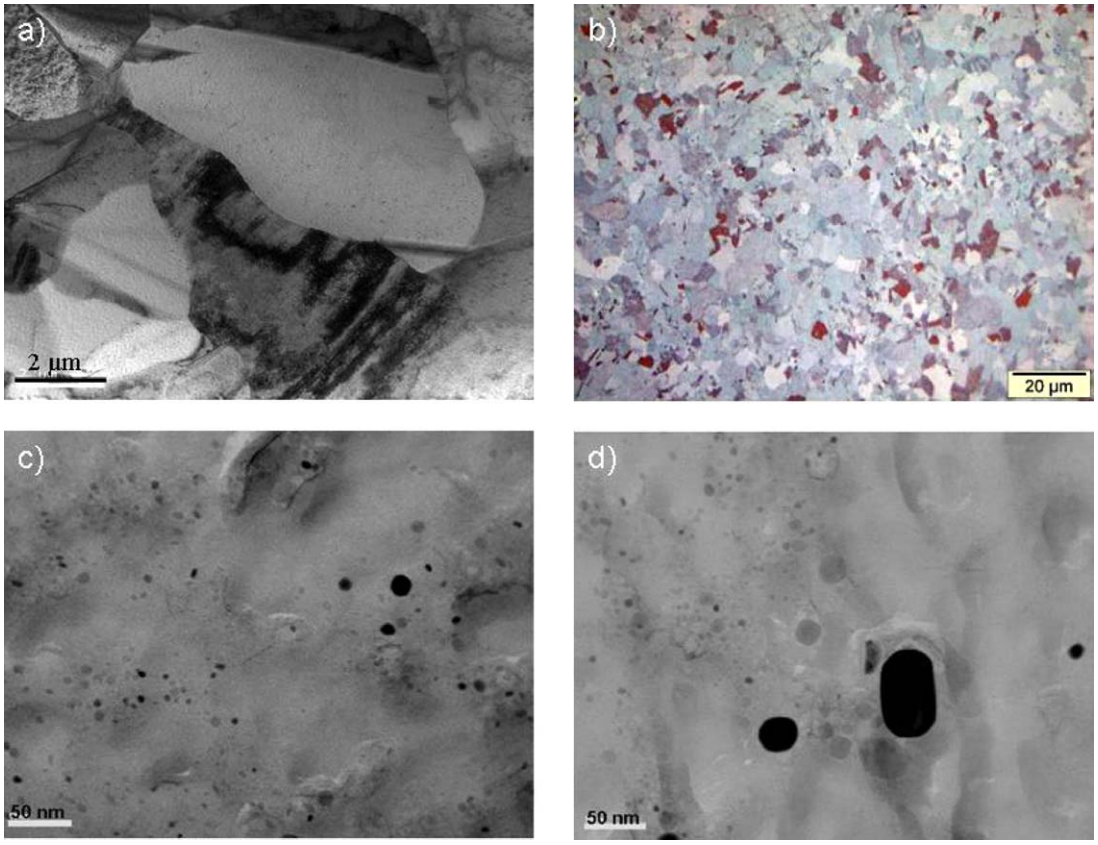

Fig. 1. Microstructural observations of sample (C). (a) Bright field TEM micrograph showing the partially recrystallised grain structure. (b) Optical micrograph (grain size 3–4 µm). (c and d) TEM extraction replicas showing the VC precipitates in black.

Sample B consisted of heavily cold rolled austenite (grain size prior to rolling 8–10 µm) which could not be usefully analysed in the TEM. However selective chemical dissolution confirmed that no V was precipitated in this specimen. Fig. 1 shows microstructural observations of sample C (with VC). Precipitation of VC slows down the recrystallisation kinetics [9] so that the final austenitic microstructure contains a few partially recrystallised grains (Fig. 1a), however the vast majority of the material is fully recrystallised. The mean grain size was 3–4 µm (Fig. 1b). The distribution and the mean radius of the VC precipitates in the sample C were determined using TEM extraction replicas. Fig. 1c and d shows VC precipitates with radii varying from 1 to 25 nm.

Fig. 2 shows the VC size distribution as measured from TEM replica observations. The average precipitate radius is 3.9 nm and the distribution can be adequately described by a log-normal function. Selective chemical dissolution followed by ICP-OES indicated that 1537 ppm wt. V was precipitated after annealing [9]. This is equivalent to a volume fraction of ~0.23% of VC.

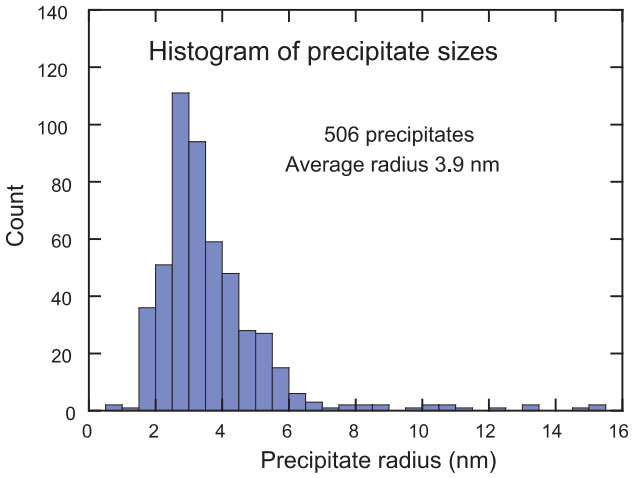

Fig. 2. VC size histogram from carbon replicas of the sample (C).

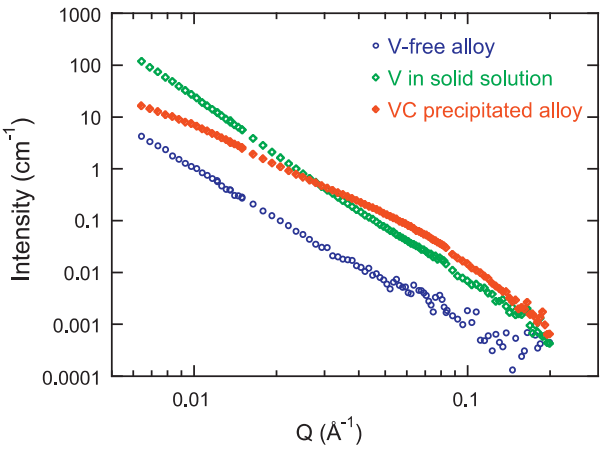

Fig. 3. *I* versus Q for the 3 reference (without H) samples. Without V (A), V in solid solution (B) and VC precipitates (C).

3.2. SANS results

3.2.1. Comparison between the initial (uncharged) microstructures

Fig. 3 shows the scattered intensities in a log–log plot for the three initial (uncharged) microstructures.

The reference sample (A) shows the lowest scattering intensity, due to the absence of any VC precipitates and the fully recrystallised microstructure. The recorded signal corresponds to the background from the matrix (scattering from remaining impurities and crystalline defects).

The full hard specimen with V in solid solution (B) shows substantial scattering at low scattering vectors. This scattering decreases linearly in the log–log plot, following a power law that will be discussed more in detail in the next section. Since this material does not contain additional precipitates as compared to sample (A),[2] it can be inferred that the measured signal is related to the high density of crystalline defects introduced by cold rolling.

The recrystallised sample containing VC precipitates (C) presents a scattering signal typical of a low volume fraction precipitate-containing matrix, with a broad shoulder. The integrated intensity of this signal Q_o (after background Laue intensity subtraction and extrapolation to infinite scattering vectors using the Porod asymptotic behaviour) provides a measurement of the precipitate volume fraction:

$$Q_o = \int_0^\infty I(Q)Q^2\,dQ = 2\pi^2 f_v(1-f_v)(\rho_p-\rho_m)^2$$

where f_v is the precipitate volume fraction, ρ_p and ρ_m are the density of neutron scattering lengths in the precipitates and matrix:

$$\rho_p = \frac{b_V + b_C}{2\Omega_p} = 3.49\times 10^{14} m^{-2},$$

$$\rho_m \cong \frac{4b_{Fe} + b_{Mn}}{5\Omega_m} = 5.77\times 10^{14} m^{-2}$$

where b_i is the nuclear (coherent) scattering length of species *i* (see Table 3), and $\Omega_p = 8.97$ Å^3 and $\Omega_m = 11.8$ Å^3 are the average atomic volumes of the precipitate and matrix.

The measured volume fraction is 0.27%, which is in good agreement with that obtained by selective dissolution presented above (~0.23%).

[2] The absence of any strain-induced precipitation was confirmed by chemical extraction followed by ICP-OES.

Table 3
Nuclear coherent scattering length.

	Fe	Mn	C	V	H
b ($1\times E^{-15}$ m)	9.4500	−3.7300	6.6460	−0.3824	−3.739

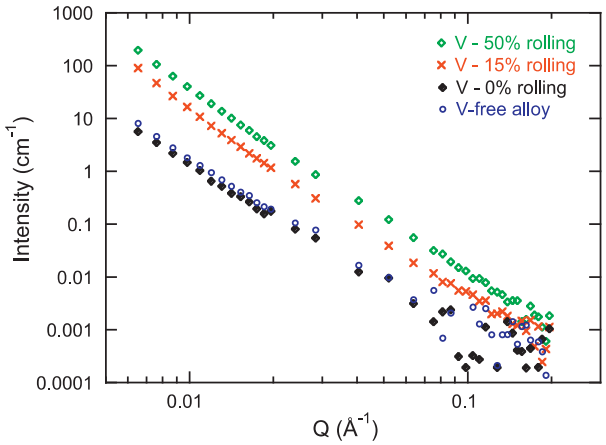

Fig. 4. *I* versus Q for the samples with V in solid solution (B) at different cold rolling reduction (0%, 15% and 50% reductions). The reference (A) annealed sample without V is included for comparison (free alloy).

From this scattering curve, we also calculated the Porod radius of the precipitate distribution using the equation below:

$$R_p = \frac{3V}{S} = \frac{3Q_o}{K\pi}$$

S and *V* are the total surface and the total volume of the precipitates, Q_o is the integrated intensity as defined above and *K* is the *Y*-intercept of $I{\cdot}q^4 = f(q^4)$ [35]. We obtained a value of $R_p = 3.3 \pm 0.2$ nm, which is consistent with the TEM measurements.

3.2.2. Effect of cold rolling reduction

The intensity of scattering from sample (B) was higher than expected. In order to further investigate the origin of this signal we measured samples with different cold rolling reductions. Fig. 4 shows the effect of variations in the amount of cold rolling reduction (0%, 15% and 50%) applied to reference sample (B) on the scattering intensity in the uncharged state (<2 ppm wt. of H). The scattering intensity of the fully recrystallised reference sample without V (sample (A)) is also included for comparison.

When no cold rolling is applied, the scattering intensity of the V-containing material is similar to that of the recrystallised, non-V containing material, showing that the presence of V in solid solution and also the difference in grain size does not have a significant effect on the neutron scattering intensity. The sample with 15% cold reduction shows a scattering intensity intermediate between that of the 0% and 50% rolled materials. It also exhibits a similar power-law scattering behaviour, with an exponent of about −3.5. This behaviour is consistent with what is known from the scattering of dislocations, which have been shown to produce a Q^{-3} behaviour [36]. The difference in scattering intensity between the three cold rolling reductions can therefore be attributed to the difference in the density of dislocations, twins and stacking faults introduced by the plastic strain.

3.2.3. Effect of H charging on the full hard sample (sample B)

We have evaluated the effect of H charging on the scattered intensity from full hard samples cold rolled to 50% reduction (V in solid solution). Fig. 5 shows the comparison at small scattering vectors of the scattering intensity from the uncharged (B) sample

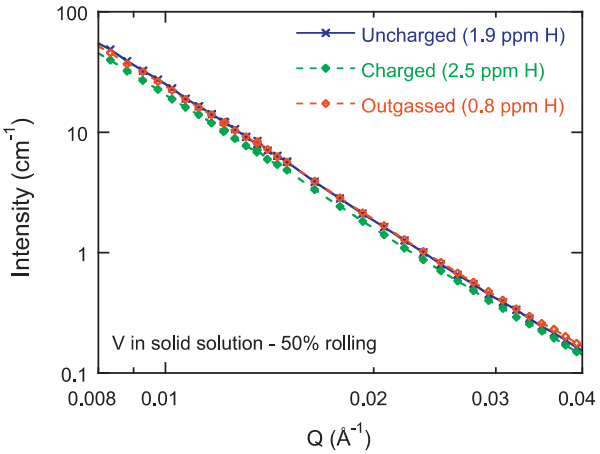

Fig. 5. *I* versus *Q*. Effect of H concentration on scattering from crystal defects of the sample (B).

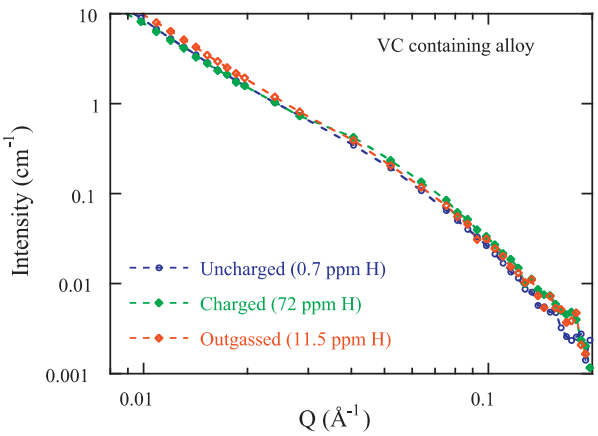

Fig. 6. *I* versus *Q* for samples (C) with VC precipitates at different concentrations of H.

(measured H content: 1.9 ppm wt.), in the same sample after H charging (measured H content: 2.5 ppm wt.) and after charging followed by outgassing by annealing under vacuum for 24 h at 260 °C (measured H content: 0.8 ppm wt.).

When the full hard sample (B) is hydrogen charged the scattering intensity decreases, while the same power law exponent is still observed. Outgassing reverses this change: the outgassed sample shows the same scattering intensity as the uncharged sample. This change of intensity occurring after H charging is likely due to the segregation of mobile H to defects that results in a decrease of the associated strain fields and therefore to the scattering intensity that is related to the magnitude of this strain field. Due to its large partial molar volume, atomic H is known to be sensitive to local stress fields [37]. The complete reversibility of the intensity change with outgassing implies that this treatment removes most or all of the H segregated to crystalline defects.

The fact that the nuclear scattering intensity decreases with the addition of H is not expected from the existing literature, e.g. Ross et al. [20]. These authors measured that the scattering intensity, associated with H-dislocation interactions in palladium, *increases* with H and *decreases* with *D*. However, besides the large difference in the H solubility in Pd and Fe–Mn–C TWIP steel, different types of defects may be present in each experiment. Moreover their calculations do not include the influence of the effect of stress relaxation due to trapped H [38]. In our case the Fe–Mn–C TWIP steels are strongly twinned and have low stacking fault energy. This low energy induces a large number of stacking faults due to the dissociation of dislocations. According to the observation of H trapping on ε martensite [25], it is anticipated that H segregation on these stacking faults also occurs.

At large scattering vectors, no effect of H is observed. This is quite reasonable because at large *Q* the crystalline defects do not contribute much to the scattered intensity.

3.2.4. *Interaction between H and the VC precipitates (sample C)*

We have evaluated the effect of H charging on sample (C) containing VC precipitates. In this case a strong charging procedure was followed, resulting in 72 ppm wt. of H in the charged sample. After outgassing for 16 h at 150 °C the remaining H concentration was 11.5 ppm wt.

Fig. 6 shows the comparison of the scattering intensity of the three samples, namely uncharged specimen (C), specimen (C) after H charging and specimen (C) after H charging and outgassing. At low scattering vectors, it is observed that the scattering intensity decreases with the addition of H, and increases with outgassing. This behaviour is similar to that observed in the full hard sample, and it can be assumed that it is representative of the interaction between H and the crystalline defects remaining in the sample. Actually, when the sample is outgassed at 150 °C the scattering intensity at low *Q* increases to values that are significantly higher than the reference sample. This is logical if we assume that there is strong outgassing of H reversibly trapped at crystalline defects but not from the residual H trapped by the VC precipitates.

At larger scattering vectors, where most of the signal relates to the VC precipitates, the opposite behaviour is found, namely the scattering intensity increases with the addition of H and decreases again with outgassing.

The intensity variations can be more easily observed in a Kratky plot of $I{\cdot}Q^2$ versus *Q* [35] (see Fig. 7). On this plot the scattering vector at the intensity maximum at the shoulder is inversely proportional to the average precipitate radius and the area below the curve is the integrated intensity that depends on the precipitate volume fraction and the scattering contrast between the precipitates and matrix. This plot shows that the addition of H strongly increases the scattering intensity (by approximately 25%). Moreover, this increase of intensity is close to a multiplication factor in the range of scattering vectors where the intensity is dominated by the signal of precipitates, since the shape of the signal is not much affected. When the sample is outgassed at 150 °C, the intensity is observed to decrease, but stays significantly higher than that of the reference sample, which is consistent with the remaining H concentration measured after degassing (11 ppm vs. 0.7 ppm in the uncharged sample).

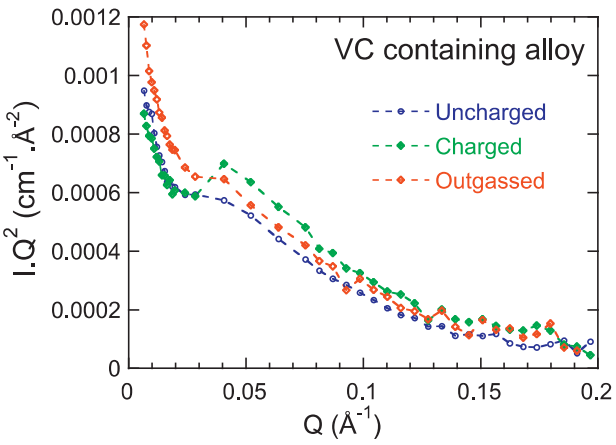

Fig. 7. Kratky plot of IQ^2 versus *Q* for samples (C) with VC precipitates at different concentrations of H.

3.2.5. Quantitative assessment of the interaction between VC precipitates and H

The change in neutron scattering intensity with H charging and outgassing observed in sample (C) demonstrates that an interaction exists between H present in the alloy and VC precipitates. The increase in neutron scattering intensity with H charging corresponds to an increase of the contrast in scattering length density between the precipitates and matrix. Since the coherent nuclear cross-section of H is negative and the precipitate scattering length density is smaller than that of the matrix, this contrast enhancement corresponds to H trapping by the precipitates. We have seen that the increase of intensity measured in the H-charged sample corresponded nearly to a simple multiplication factor of the reference (uncharged) sample signal. This experimental data is consistent with a homogeneous trapping of H inside the precipitates, although it is not possible to rule out a heterogeneous trapping of H in the vicinity of the precipitate–matrix interface. H trapping of TiC particles in bcc steels has been shown to occur both at the particle/matrix interface and in the bulk and to depend on the coherency of the precipitate/matrix interface [39]. Moreover H trapping in the bulk of semi-coherent and incoherent γ′ (Ni_3Al) precipitates in fcc Ni base superalloys has been evidenced by tritium autoradiography [40]. Atomistic calculations have shown that such a H segregation in Ni_3Al precipitates is the result of a larger H solubility in the Ni_3Al phase than in Ni base matrix [41]. Similar effects may explain H trapping in the bulk of VC precipitates.

Within this hypothesis, we can evaluate the relationship between the trapped H content in the precipitates and the change in neutron scattering intensity.

For a two-phase system, the neutron scattering intensity $I(Q)$ is proportional to the square of the contrast in nuclear scattering density [35]:

$$I(Q) \propto (\rho_p - \rho_m)^2$$

The effect of H on the nuclear scattering length of the matrix can be neglected since the H concentration is very low so that:

$$\rho_m \cong \frac{4b_{Fe} + b_{Mn}}{5\Omega_m}$$

To calculate the effect of H intake in the precipitates, we will use the approximation that the lattice parameter of the VC precipitates is not changed significantly by the presence of H. We will define the fraction X_{pH} of H inside the precipitates as the ratio between the number of H atoms and half the number of (V + C) atoms:

$$X_{pH} \cong \frac{2n_H}{n_V + n_C}$$

Then the nuclear scattering length density of the precipitates becomes:

$$\rho_p \cong \frac{(1/2)b_V + (1/2)b_C + X_{pH}b_H}{\Omega_p}$$

The fraction of H in the precipitates X_{pH} can be translated into the overall concentration of H in the sample that is trapped in the precipitates (X_{totH} in atomic fraction):

$$X_{totH} = f_v \frac{\Omega_m}{\Omega_p} X_{pH}$$

And finally the overall concentration of H in the sample C_{totH} trapped in the precipitates can be expressed in ppm wt.:

$$C_{totH} = \frac{10^6}{55.4} X_{totH}$$

With the above equations we can relate the relative change in scattering intensity $\Delta I/I$ to the amount of H trapped inside the precipitates (expressed as an overall H concentration in the sample).

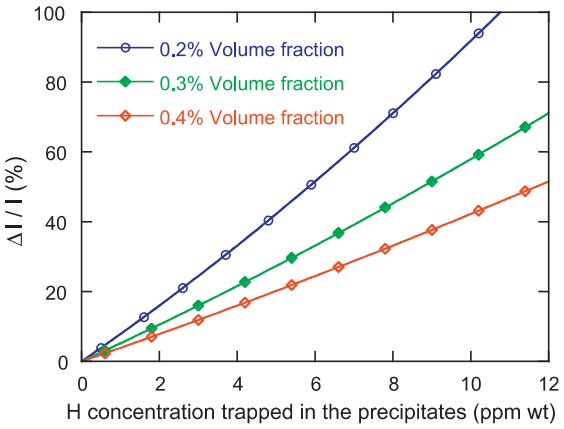

Fig. 8. $\Delta I/I$ versus concentration of H trapped in the VC precipitates.

Fig. 8 shows a plot of this relative variation of intensity for different values of the precipitate volume fraction.

Experimentally, it is difficult to obtain a precision in intensity calibration that is better than 10–15% in SANS data, so that it is unlikely that, for the precipitate volume fractions investigated in this work, H trapping quantities corresponding to an overall concentration of less than 2 ppm wt. can be detected with this technique.

The relative increase in neutron scattering intensity observed after strong H charging in alloy (C) (see Fig. 7) is about 25%. Therefore there should be about ~5 ppm wt. of H trapped inside the precipitates (assuming 0.3% volume fraction of VC). The vast majority (67 ppm wt. H) must therefore be segregated to crystalline defects and grain boundaries or homogeneously distributed in the matrix.[3] 5 ppm wt. of H trapped in a volume fraction of about 0.3% corresponds to an atomic fraction of H in the precipitates of about 10%. After vacuum outgassing at 150 °C the scattering intensity decreases. $\Delta I/I$ is about 12% more than the reference sample which suggests that there remains ~3 ppm wt. of H trapped in the precipitates after outgassing. Thus, it appears that the VC precipitates are reasonably effective irreversible H trapping sites for moderate H concentrations, up to a few ppm wt. From the data analysis carried out in the present work, the H trapping appears to occur homogeneously within the precipitates.

4. Conclusion

In this work we have studied the interaction between H and an austenitic Fe–Mn–C TWIP steel containing V with different microstructures using TEM and SANS. The main conclusions that can be drawn from this experimental study are the following:

- No interaction between H and V in solid solution has been detected.
- A significant interaction between H and structural defects introduced by plastic deformation (cold rolling) has been measured. Namely, the neutron scattering intensity related to these structural defects was lowered by the introduction of H in the samples. This is possibly due to a reduction in the strain field of the partial dislocations due to the segregation of H. This effect was reversible upon outgassing.
- A significant interaction between H and VC precipitates has been measured. Namely, an increase of the neutron scattering intensity is observed when the samples are charged with H. From the

[3] No signs of damage or macroscopic H_2 gas blistering were seen.

intensity increase this is consistent with the homogeneous trapping of H within the precipitates rather than at the precipitate/matrix interface. In the studied conditions, we have shown that approximately 5 ppm wt. of H could be trapped in this way. This effect was not completely reversible upon sample outgassing at 150 °C, showing that the VC precipitates are moderately stable H trapping sites.

Acknowledgements

The authors would like to thank C. Dewhurst and D. Bowyer on D11 at ILL, A. Radulescu on KWS-2 at the Julich Neutron Centre for their instrumental helps and G. Petitgand and P. Barges from ArcelorMittal for their experimental works. We also acknowledge VANITEC for their financial contribution.

References

[1] C. Scott, S. Allain, M. Faral, N. Guelton, Rev. Metall. 103 (2006) 293.
[2] J.K. Kim, L. Chen, H.S. Kim, S.K. Kim, Y. Estrin, B.C. De Cooman, Metall. Mater. Trans. A 40A (2009) 3147.
[3] G. Frommeyer, U. Brüx, P. Neumann, ISIJ Int. 43 (2003) 438.
[4] H. Idrissi, K. Renard, L. Ryelandt, D. Schryvers, P.J. Jacques, Acta Mater. 58 (2010) 2464.
[5] O. Grässel, L. Krüger, G. Frommeyer, L.W. Meyer, Int. J. Plast. 16 (2000) 1391.
[6] A. Dumay, J. Chateau, S. Allain, S. Migot, O. Bouaziz, Mater. Sci. Eng. A 483–484 (2008) 184.
[7] A. Zinbi, A. Bouchou, Mater. Design 31 (8) (2010) 3989.
[8] S. Yamasaki, T. Takahashi, Tetsu-to-Hagane 83 (7) (1997) 454.
[9] C. Scott, B. Remy, J.-L. Collet, A. Cael, C. Bao, F. Danoix, B. Malard, C. Curfs, Int. J. Mater. Res. (formerly Z. Metallkd.) 102 (2011) 5.
[10] K. Takai, H. Shoda, H. Suzuki, M. Nagumo, Acta Mater. 56 (2008) 5158.
[11] T. Ohmisawa, S. Uchiyama, M. Nagumo, J. Alloys Compd. 356–357 (2003) 290.
[12] E. Tal-Gutelmacher, D. Eliezer, E. Abramov, Mater. Sci. Eng. A 445–446 (2007) 625.
[13] K. Ebihara, T. Suzudo, H. Kaburaki, K. Takai, S. Takebayashi, ISIJ Int. 47 (2007) 1131.
[14] Y. Su, Y. Tomota, J. Suzuki, M. Ohnuma, ISIJ Int. 51 (9) (2011) 1534–1538.
[15] A. Oudriss, S. Frappart, I. Legrand, J. Bouhattate, J. Creus, C. Savall, X. Feaugas, in: L. Duprez (Ed.), Steely Hydrogen Conference Proceedings, OCAS, Ghent, Belgium, 28–29 September, 2011.
[16] J. Chêne, in: L. Duprez (Ed.), Steely Hydrogen Conference Proceedings, OCAS, Ghent, Belgium, 28–29 September, 2011.
[17] Y. Nishiyama, P. Langan, H. Chanzy, J. Am. Chem. Soc. 124 (31) (2002) 9074.
[18] H. Sakaguchi, A. Kohzai, K. Hatakeyama, S. Fujine, K. Yoneda, K. Kanda, T. Esaka, Int. J. Hydrogen Energy 25 (12) (2000) 1205.
[19] M. Zanarini, P. Chirco, M. Rossi, G. Baldazzi, G. Guidi, E. Querzola, M.G. Scannavini, F. Casali, A. Garagnani, A. Festinesi, Nuclear Sci. 42 (4) (1995) 580.
[20] D.K. Ross, K.L. Stefanopoulos, K.S. Forcey, I. Iordanova, Z. Phys. Chem. 183 (1994) 29.
[21] M. Maxelon, A. Pundt, W. Pycknout-Hintzen, J. Barker, R. Kirchheim, Acta Mater. 49 (2001) 2625.
[22] C. Kluthe, T. Al-Kassab, J. Barker, W. Pycknout-Hintzen, R. Kirchheim, Acta Mater. 52 (2004) 2701.
[23] A. Ulbricht, J. Böhmart, M. Uhlemann, G. Müller, J. Nucl. Mater. 336 (2005) 90.
[24] M. Ohnuma, J. Suzuki, F. Wei, K. Tsuzaki, Scripta Mater. 58 (2008) 142.
[25] J. Chêne, J. Ovejero Garcia, C. Paes de Oliveira, M. Aucouturier, P. Lacombe, J. Microsc. Spectros. Electron. 4 (1979) 37.
[26] A.M. Brass, J. Chêne, in: T. Magnin (Ed.), 2nd Int. Conf. on Corrosion – Def. Interactions, vol. 21, The Inst. of Mater. for the Eur. Fed. of Corrosion, Nice, France, 1996, p. 196.
[27] P. Bastien, P. Azou, C. R. Acad. Sci. 232 (1951) 1845.
[28] J.A. Donovan, Metall. Trans. A 7A (1976) 1677.
[29] A.M. Brass, J. Chêne, Mater. Sci. Eng. A 242 (1998) 210.
[30] J. Chêne, A.M. Brass, Scripta Mater. 40 (1999) 537.
[31] F. Lecoester, J. Chêne, D. Noel, Mater. Sci. Eng. A 262 (1999) 173.
[32] A. Dumay, Ph.D. at the Institut National Polytechnique de Lorraine, 2008, http://pegase.scd.inpl-nancy.fr/theses/2008_DUMAY_A.pdf.
[33] C. Sykes, H.H. Burton, C.C. Gegg, J. Iron Steel Inst. 156 (1947) 155.
[34] T. Dieudonné, L. Marchetti, F. Jomard, M. Wery, J. Chêne, C. Allely, P. Cugy, C. Scott, JJC, Presses des Mines, 2011, p. 17.
[35] O. Glatter, O. Kratky, Small Angle X-ray Scattering, Academic Press Inc., London Ltd., 1982.
[36] J.E. Epperson, B.A. Loomis, J.S. Lin, J. Nucl. Mater. 108 (1982) 476.
[37] A.-M. Brass, J. Chêne, J. Phys. IV France 09 (1999) 4.
[38] M. Can Uslu, D. Canadinc, J. Mater. Sci. 45 (2010) 1683.
[39] F.G. Wei, K. Tsuzaki, Metall. Mater. Trans. A 37 (2) (2006) 331.
[40] D. Roux, J. Chêne, A.-M. Brass, in: A.W. Thompson, N.R. Moody (Eds.), Hydrogen Effects in Materials, TMS, Warrendale, PA, 1996, p. 923.
[41] M.I. Baskes, J.E. Angelo, N.R. Moody, in: A.W. Thompson, N.R. Moody (Eds.), Hydrogen Effects in Materials, TMS, Warrendale, PA, 1996, p. 77.